Influences of Tides, Winds, and Bathymetry on Surface Transport Through a Complex Nearshore System: Measurements from GPS Drifters and an Uncrewed Aerial Vehicle

Andrew Robinson[1] · Charles Tilburg[1]

Abstract

Bathymetric features such as dredged channels, constricted-inlet basins, and nearshore islands have known influences on coastal transport, which are typically studied on an individual basis. However, their interactive effects on flow when found in the same area are poorly characterized. A multi-season study was conducted to characterize surface transport in and around Wood Island Harbor, in the southwestern Gulf of Maine, where these features all exist in close proximity. Patterns of surface transport were assessed with repeated series of Uncrewed Aerial Vehicle flights and deployments of GPS drifters across tidal conditions and winds typical to the area. Transport followed a major axis through the harbor, as a result of the combined effects of the linked inlet-channel system. Despite the complex topography, the individual dynamics of transport are maintained. Tidal variations explained a majority of displacement ($R^2 = 0.752$) along the channel axis, while across-channel wind velocity explained the majority of orthogonal displacement ($R^2 = 0.646$). Flow in the area was friction-dominated, and both inter-island passages and the deep channel served to direct flow. The offshore transport of tidally driven flows from a constricted-inlet basin was enhanced by deep channels, with flow primarily following bathymetric contours. Our observations suggest that surrounding topography lessened the role of wave energy in governing transport. The co-occurrence of bathymetric features around a constricted-inlet basin can disrupt the typical influences of physical mechanisms on surface transport, leading to a greater importance of local conditions and the larger-scale circulation of the area.

Keywords Constricted-inlet basin · Tidal exchange · Nearshore circulation · Complex bathymetry · Uncrewed Aerial Vehicle (UAV) · Drifters

Introduction

Complex topographical and bathymetric features are common in the nearshore environment, exerting strong influences on local current regimes. While the particular structure of a region ultimately determines its current dynamics, some unifying patterns of flow have been described for features such as constricted-inlet basins (e.g., Zarzuelo et al. 2017; de Ruiter et al. 2019), dredged channels (e.g., Lee et al. 2013; Chen et al. 2015), and inter-island passages (e.g., Brooks 2004).

Although the body of past work considers the effects of each of these structures individually, the interaction of these features in a single geographical area remains unexplored. Here, surface transport between a constricted-inlet basin and a coastal bay was investigated. The exchange between these bodies of water occurs through a harbor containing a dredged navigational channel that is surrounded by multiple islands, both features that may modify flow.

Constricted-inlet basins exhibit some unifying conditions of flow, both within their boundaries and in their exchange with the ambient ocean. Close to the mouth of the basin, tidal currents through the inlet are the primary mechanism governing patterns of flow (Zarzuelo et al. 2017). During a flood tide, water is drawn into the basin from a fan-shaped region immediately surrounding the channel mouth. The surface area from which water is drawn is large relative to the cross-sectional area of the inlet, producing swift currents through the channel and a focused, jet-like flow directed into the basin

✉ Andrew Robinson
arobinson15@une.edu

[1] School of Marine & Environmental Programs, University of New England, 11 Hills Beach Road, Biddeford, ME 04005, USA

(Lee et al. 2013; Rynne et al. 2016). On the ebb tide, the pattern is reversed, with concentrated flow directed out of the basin. In both cases, current speed decreases with distance from the inlet, as the flow broadens while still proceeding along the same axis of the channel (Baines 1957; Maas 1997; de Ruiter et al. 2019). As the ebb jet moves offshore, it can interact with larger flow patterns of the region. In areas where the outflow from a basin merges with a coastal current, water is exported more efficiently, enhancing the flushing of waters over successive tide cycles (DiLorenzo et al. 1995; Viero and Defina 2016). While not considered in this investigation, the bathymetry of constricted-inlet basins also influences flows within the basin, modifying the tidal response, spatiotemporal variation in currents and shear stresses, flushing, and sediment transport (e.g., Krüger and Healey 2006; Stanev et al. 2007; Hunt et al. 2016; Zarzuelo et al. 2017; de Ruiter et al. 2019).

The strong currents into and out of constricted-inlet basins are often associated with high levels of shear, resulting in turbulence as energetic flow interacts with the bounds of the coastline and seafloor (Hamner and Hauri 1977; Brooks 2004; Lee et al. 2013; Hunt et al. 2016; Zarzuelo et al. 2017; de Ruiter et al. 2019). Horizontal shear is found near the edges of the inlet, often producing eddies of varying spatiotemporal scales both within and downstream of the inlet (Krüger and Healy 2006; Lee et al. 2013; Zarzuelo et al. 2017; de Ruiter et al. 2019). Lee et al. (2013) found that eddy production can be enhanced by obstacles within the inlet or when the constriction is sharp or abrupt relative to the surrounding coastline. The turbulence in flow through constricted inlets varies within tidal cycles and over longer time scales. Velocities vary between slack tide and peak flow, and spring tides tend to generate faster currents, as a greater volume must pass through the inlet in the same amount of time. Stronger currents during such periods lead to considerably more energy dissipation (Zarzuelo et al. 2017; de Ruiter et al. 2019). With increased turbulence, more rapid attenuation of the jet-like tidal current on the downstream side of the inlet would occur (Zarzuelo et al. 2017).

Dredged channels often exhibit flow dynamics similar to tidal inlets, especially when large differences exist between the depth of the channel and the surrounding waters (Chen et al. 2015). When dredged channels run through shoal areas, flow in the region is directed by bathymetric contours and concentrates within the channel. Friction through the water column is reduced in deeper waters, as the friction-dominated bottom boundary layer makes up a smaller proportion of the water column (Lee et al. 2013; Chen et al. 2015). As a result, energetic and swift currents are created through the channel, while weak flows continue over shoal areas. When a constricted-inlet basin is associated with a dredged channel, their cumulative effects in directing flow may further amplify ebb currents flowing out of the basin. However, like an ebb jet out

of a basin, the high-velocity flow through a dredged channel can rapidly attenuate moving offshore (Chen et al. 2015).

Flow instability also results when currents interact with offshore islands. When such an obstacle in the ocean bifurcates a current, energy is attenuated by friction, and a region of instability is created in the direct lee, known as the island wake effect (e.g., Wolanski et al. 1984). Paired eddies can form, causing local water retention and a decrease in velocity of the currents flowing on either side (Wolanski et al. 1984; Signell and Geyer 1991; Brooks 2004). When multiple islands are present close to one another, flow may be channeled through an inter-island passage, instead of being split when meeting an island head-on. However, strong currents through inter-island passages are still likely to create shear and turbulence, spawning eddies that can variably induce dispersion or retention of water (Hamner and Hauri 1977; Brooks 2004; Krüger and Healy 2006; Lee et al. 2013). When the currents are tidally driven, eddies typically do not persist once the tide changes (Wolanski et al. 1984), although the islands still influence flow over smaller time scales in the ways described above.

Physical processes through the air-sea interface can interact with the influences of these topographic features, introducing further complexities to the flow. Wind, especially along the primary axis of a constricted inlet, can either enhance, attenuate, or re-direct flow. If the direction of tidal flow is aligned with the wind, current velocities will increase, primarily in the surface layer. However, winds oriented across the channel or opposed to the direction of the tidal current create friction at the surface, resulting in reduced current speeds or across-channel displacement (Zarzuelo et al. 2017). With a sufficiently strong wind forcing, flow in the surface layer can be reversed from the prevailing tidal current. This flow reversal not only reduces the mass transport in or out of the basin but creates turbulence and vertical shear, stimulating mixing while lessening the energy and speed of the tidal current (Ralston and Stacey 2006). Waves interacting with currents through a dredged channel can enhance offshore flow through wave setup along the coast (Chen et al. 2015; Moulton et al. 2017) or attenuate high-velocity transport through the channel. Our study sought to characterize the effects of these interacting mechanisms on a constricted-inlet basin that exchanges with the surrounding ocean through a complex harbor.

The basin selected for this study, Biddeford Pool, is linked with the Gulf of Maine (NE, USA) through Wood Island Harbor and Saco Bay. While the hydrography of Biddeford Pool has only received limited study (e.g., Reynolds and Casterlin 1985; van Heteren et al. 1996), the flow patterns in the surrounding area are described more thoroughly. This body of work was used to inform expectations for the flow regimes through the area. Currents around this region exhibit short-term and seasonal

variability, across multiple spatial scales (Bigelow 1927). Along the offshore extent of the study area, the Western Maine Coastal Current (WMCC) flows southwestward, forced by seasonally moderated river discharge along the Maine coast (Geyer et al. 2004; Churchill et al. 2005; Pettigrew et al. 2005). Within Saco Bay, surface circulation is anticyclonic, with northward flow close to shore and flow parallel to the WMCC offshore (Moore et al. 2020).

Circulation through the area is also subject to the influence of wind and wave conditions, which interact with the complex topography of Wood Island Harbor, in southern Saco Bay. Wind stress alters the offshore extent of the Saco River plume and WMCC (Geyer et al. 2004; Tilburg et al. 2011; Fortier 2014) and in extreme cases can cause a reversal in surface circulation (Geyer et al. 2004; Moore et al. 2020). Discharge from the Saco River supplies sediment to the area, which is then distributed by seabed currents on a seasonal basis, moderated by wind and storm patterns (Hill et al. 2004; Kelley et al. 2005; Brothers et al. 2008). The islands surrounding Wood Island Harbor are known to modify the influence of winds and wave action on the currents of Saco Bay (Kelley et al. 2005; Hill et al. 2004). It was therefore expected that they would modify the surface transport in and out of Biddeford Pool, altering the typical patterns of exchange for constricted-inlet basins. Understanding flow through complex nearshore systems is of both practical and ecological significance. Natural processes of sediment erosion and accretion in these areas can come into conflict with human activities, requiring intervention. Within Biddeford Pool, sediment from the Saco River (average 895 m^3 year^{-1}) accumulates in the channel and basin, requiring periodic dredging by the US Army Corps of Engineers (USACE) (Kelley et al. 2005; Brothers et al. 2008; USACE 2016). Measuring flow in advance of dredging in the 2020–2021 winter (USACE 2020a, c) allows for later assessments of its effects on the exchange of the basin.

The dependence of constricted-inlet basins on tidal flushing through a narrow opening makes them more susceptible to compromised water quality (Viero and Defina 2016). In Biddeford Pool, high levels of sewage-associated microbes in recent years have led to the closure of the softshell clam fishery (Graham 2019), valued at a peak of $260,083 in 2016 (Maine DMR 2020). Fecal pollution can also cause a decrease in the diversity of existing aquatic microbes (Paruch et al. 2019), an important community in salt marsh habitats like those found on the margins of tidal basins. The Saco River represents a potential source of these microbial pollutants (Tilburg et al. 2015), but river discharge has not been linked to the waters of Biddeford Pool. Understanding the exchange of waters in a constricted-inlet system can inform investigations of pollutant sources and persistence and direct remediation efforts.

The flow dynamics generated as currents interact with a variety of co-occurring bathymetric features and physical mechanisms are more complex than what could be predicted by studies of each phenomenon individually. For instance, the extent to which transport in and out of a constricted-inlet basin is modified by a connecting channel is unknown. Additionally, topography that shelters the harbor from the coastal ocean may have a disruptive effect on wind stress or wave energy, reducing their impacts on surface flow out of the basin. Therefore, it is necessary to directly study currents in such areas to determine the causes of the observed flow and identify the controlling mechanisms. The primary aims of this study were to characterize surface transport of waters from a constricted-inlet basin through a topographically complex harbor and to identify the mechanisms influencing those patterns. Our observations were then interpreted in relation to the system of a constricted-inlet basin, a dredged channel, and islands around the harbor, allowing a more complete description of how currents are affected by the confluence of these features.

Before undertaking any sampling, previous studies in the area and the known dynamics around complex coastal features were considered to form hypotheses as to the patterns of surface transport and influencing mechanisms we expected to observe. It was anticipated that tidal flow would be the primary driver of transport through the Biddeford Pool-Wood Island Harbor system, with flow coarsely directed by dredged channels and inter-island passages. Swift currents and efficient export of water were expected on the ebb tide, as flow out of the basin follows directly into the channel of the harbor. Winds and waves were thought to be secondary influences, along with bathymetrically driven shear. Along-channel winds aligned or opposed to the direction of flow were expected to enhance or suppress transport, respectively. Ebb flows were expected to be transported offshore and out of the region, with a limited portion of the water returning to the basin on the flood tide. Inflow from the Saco River to Biddeford Pool was only expected during times of peak discharge and with winds blowing towards the coast. Variation in tidal range and wind speed was expected to alter the strength of these mechanisms in governing surface currents.

Methods

Study Area

The investigation described here was centered around Wood Island Harbor, which connects Biddeford Pool, a constricted-inlet basin, to Saco Bay and the Gulf of Maine (Fig. 1). Biddeford Pool is a shallow, irregularly shaped basin measuring 2.5 km × 1.5 km along its principal axes, bound by two tombolo complexes. Biddeford Pool lacks substantial freshwater inputs, so all water is exchanged

through a constricted inlet, measuring 40 m across. Tidal range in the area is 2.7 m (Moore et al. 2020), and the majority of Biddeford Pool drains on the ebb tide, revealing broad mudflats cut by narrow, flooded channels. An anchorage area close to the inlet is maintained for commercial and recreational vessels, with a maximum depth of 10.1 m at mean lower low water (MLLW) (USACE 2020b). The inlet leads out into a 3-m dredged channel that runs southwest to northeast through Wood Island Harbor.

Wood Island Harbor is bound on the western and southern edges by the mainland and is partitioned from Saco Bay by rocky islands. Vessel traffic out of the harbor follows two

deep natural passages: to the north between Stage and Wood Islands or to the east between Wood and Gooseberry Islands. The Saco River empties into Saco Bay immediately to the north of Wood Island Harbor.

A variety of techniques were utilized to assess patterns of surface transport through the Biddeford Pool constricted-inlet system. Data collection occurred in Wood Island Harbor between July 2019 and November 2020, with a suspension of sampling from December 2019 to February 2020 and April to June 2020. Deployments targeted combinations of tidal range, tidal direction, and wind direction. Classification of spring and neap tides was made relative to the mean tidal

Fig. 1 Map of southern Saco Bay, including Biddeford Pool, Wood Island Harbor, Saco River, and relevant topographical features. The inset map shows the study location relative to the Gulf of Maine and National Data Buoy Center Station 44007
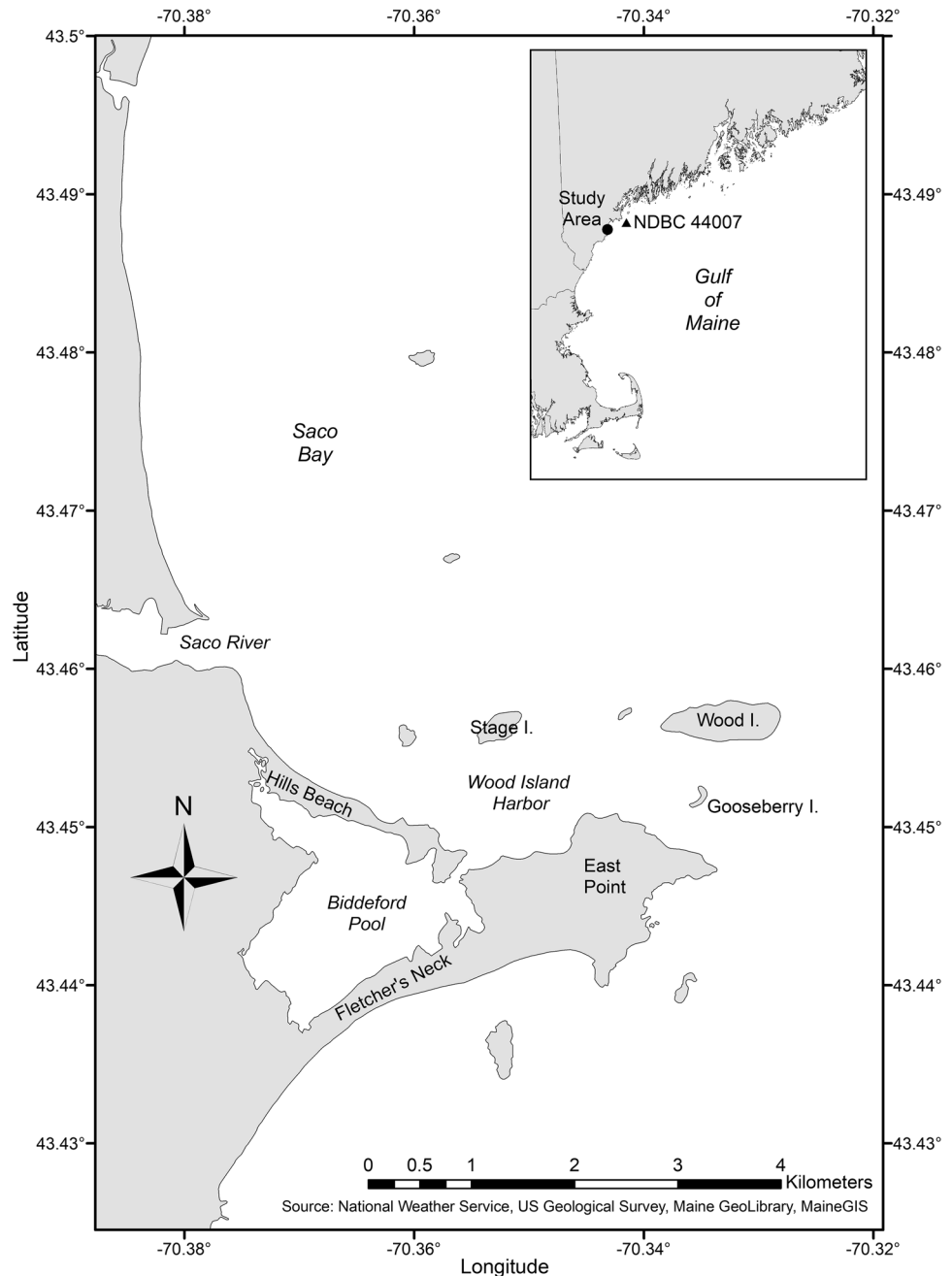
range (2.7 m). Along-channel winds were considered when planning the deployments, as the prevailing wind directions in the area (northeasterly and southwesterly) (Fortier 2014) are approximately aligned with the axis of the Biddeford Pool inlet. However, the categories of wind direction were revisited when analyzing drifter data, based on the patterns of surface transport that emerged under different wind conditions.

UAV Surveys

We assessed broad patterns of relative current direction and spatial variability in flow through Wood Island Harbor with aerial imagery captured by an Uncrewed Aerial Vehicle (UAV), specifically a Phantom 4 quadcopter drone (SZ DJI Technology Co.). Raster data from UAVs have been previously used to calculate current velocities using particle-tracking algorithms and as qualitative supplements to other methods for describing surface flow (Tauro et al. 2016; Benassai et al. 2017; Dérian and Almar 2017). The orientations of boats moored in the harbor were used as indicators of relative current direction, without calculating magnitude. Currents flowing past small boats at single-point moorings produce tension in the mooring line, driving yaw, or rotational motion (Wang et al. 2007; Hollyhead et al. 2017). However, winds can influence motion about a mooring (Wang et al. 2007), preventing us from using these data for absolute current direction and making direct comparisons with the drifter data. Sampling was conducted over the 8 sets of tidal and wind conditions originally used to group drifter deployments (ebb or flood tidal direction, spring or neap tidal range, and northeasterly or southwesterly winds). Short flights (~5 min) were conducted to capture images once every half hour over the course of a full ebb or flood tidal cycle.

GPS Drifters

To more rigorously describe current dynamics, the trajectories of flow into and out of Biddeford Pool were measured by releasing radio-tracked Lagrangian surface drifters recording location with a global positioning system (GPS) receiver. A low-profile drifter body was chosen for the shallow, complex environment, and it was paired with an electronics unit that internally logged and remotely transmitted data, using low-power radio communication (Robinson et al. 2021). Drifters were released in groups of 2–7 units and collected data for 1–4 h over a single ebb or flood tidal cycle. Deployments were terminated by either recovery on the research vessel or by grounding onshore. The integrated Arduino controller logged GPS location every 5 s when deployed, and those data were later used to calculate displacement and current velocities.

Externally Sourced Environmental Data

Measurements of wind direction and speed and wave height and direction were sourced from National Data Buoy Center Station 44007 in Casco Bay, Maine, located 20 km northeast of our study area (Fig. 1 inset). The US Geological Survey flow gauge in Cornish, Maine (Station 01066000) was used to calculate river discharge for the Saco River, using the drainage area correction established by Tilburg et al. (2011). Determinations of spring and neap tides for classifying drifter deployments and UAV flights were made using the National Oceanic and Atmospheric Administration tables published for Camp Ellis, Saco River, Maine (Station ID 8418606). Water levels during deployments were obtained from the Portland, Maine tide station (ID 8418150). Both stations provide data measured against the MLLW datum. Bathymetry data layers were obtained for the Gulf of Maine at 4 m and 8 m resolution from the University of New Hampshire Joint Hydrographic Center/Center for Coastal and Ocean Mapping.

Data Analysis

UAV data were primarily analyzed graphically, as this method was most conducive to assessing spatial variation. Using a projective transformation in ArcMap 10.7 (esri), images were corrected to a geographic coordinate system. The current direction was then estimated based on the bow and stern location of each boat. The evolution of relative flow patterns over a tidal cycle was considered for each combination of wind and tide conditions.

Current velocities and overall displacement were calculated for each drifter released. Regression analysis was then used to determine the major axis along which flow through Wood Island Harbor occurred. The wind and wave parameters listed above were averaged over the duration of each deployment. River discharge was averaged over a 48-h period preceding each deployment, as the flow response at the Saco River mouth lags 1–2 days behind the discharge measured at the Cornish gauge (Tilburg et al. 2011). To mitigate any correlation between observations from drifters deployed together, displacements and environmental parameters were averaged for the deployment as a whole. These mean values were used to calculate correlations between the variables and the displacement parallel and orthogonal to the calculated major axis.

The most informative relationships were used to construct a linear regression model of displacement through the area, given a starting location and set of wind and tidal conditions. This model was created to identify and illustrate the primary mechanisms of flow, not to replicate or predict the flow (e.g., Tilburg and Garvine 2004). However, multiple

linear regression models were fitted to the data to explore interactions and unexplained variation. Significant factors were identified with partial F-tests of main and interactive effects. To aid in our description of current dynamics, non-dimensionalized flow parameters were calculated for typical flows through the inlet and harbor. These results and the scales and assumptions used in their calculation are provided in the Online Resource.

When considering the bathymetric influences and fine-scale motions captured by the drifters, we individually examined sets of deployments within and between wind and tidal conditions. Patterns evident across multiple deployments were associated with conditions shared by those deployments to provide a more complete characterization of flow. Common trends in flow between the UAV and drifter-based sampling were investigated through data visualization.

Results

UAV Flights

Data from aerial surveys were used to capture spatial variation in relative current direction over Wood Island Harbor. Close to slack tides, surface flow was largely uniform and aligned with the wind direction. More complex patterns emerged around peak tidal flow, with distinct behavior associated with particular regions of the harbor. In Fig. 2, we present calculated current directions across the area in which boats were moored for peak tidal flow under combinations of wind and tidal directions. Plots of ebb current direction (Fig. 2a, b) revealed spatial variation through the harbor. Close to Biddeford Pool and within the channel, flow was directed offshore along the channel axis, regardless of wind direction. Winds directed into the basin produced flow into the channel from its margins (Fig. 2a). In the shallow area of the harbor (west of the channel), ebb surface currents were aligned with the wind for both conditions sampled. A similar alignment was observed during flood tidal flow across the harbor with winds blowing from offshore, as in Fig. 2c. Examination of flood currents under offshore-directed winds (Fig. 2d) revealed a division of flow through the area. Flow in the southern portion of Wood Island Harbor tended towards Biddeford Pool, while flow across the northern region of the harbor was northwestward towards Hills Beach and the Saco River.

The distributions of current direction under different combinations of wind and tide conditions (Fig. 3) provided a secondary means to evaluate the influence of these variables on flow patterns. When wind and tidal direction were aligned (Fig. 3b, c), flow tended to proceed in the direction of both winds and tidal flow. When the two mechanisms' directions were opposed (Fig. 3a, d), current directions were more variable, with at least a twofold increase in the standard deviation of the distributions. The observed effects differed across conditions of tidal range, wind direction, and position in the harbor. Northeasterly winds were associated with southwestward currents over much of the harbor on the ebb tide (Fig. 3a). However, northeastward flow was maintained in the channel for both spring and neap tide. Distributions of flood current directions under southwesterly winds (Fig. 3d) were not consistent across differing tidal ranges. Under spring tides, a bimodal distribution of flow was observed, reflecting the divergence of surface transport towards Biddeford Pool and the Saco River observed in Fig. 2d. Neap tidal flow was more uniform but did not align

Fig. 2 Current direction vector fields at peak tidal flow across Wood Island Harbor under spring tides, for combinations of wind and tidal directions. Arrows are colored by northeasterly and southwesterly winds. Note that the arrows indicate direction only. Wind velocity is indicated by the arrow in the top right corner of each panel
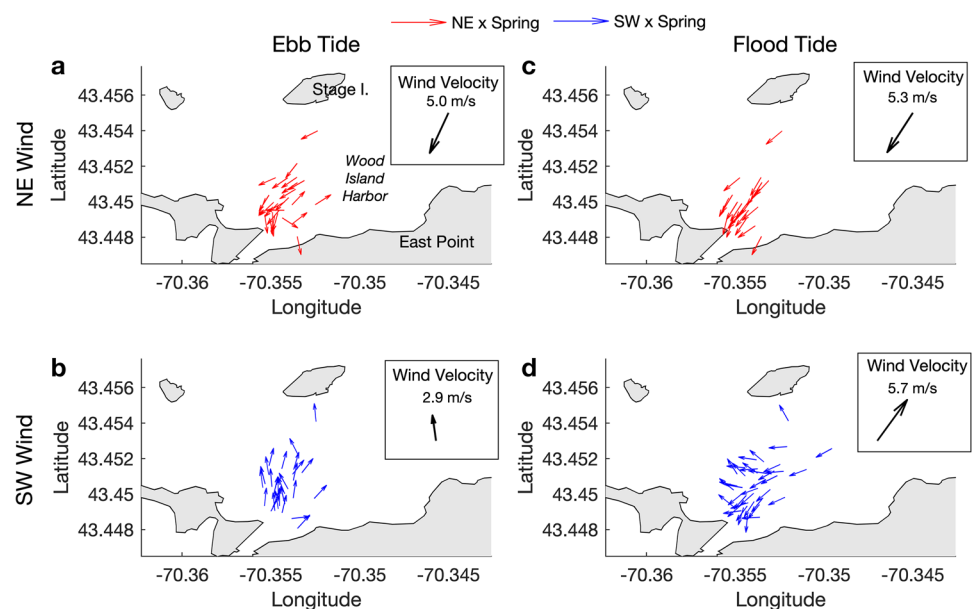
Fig. 3 Relative frequency distributions of current direction in degrees true (0° = northward) within 15-degree bins, pooled across 3 flights centered around mid-tide for each day of UAV operations. Data are divided between ebb (**a**, **b**) and flood (**c**, **d**) tidal conditions and north-easterly (**a**, **c**) and southwesterly (**b**, **d**) wind directions. The number of boats in the harbor (i.e., datapoints) varied between 20 and 40 across the flights from which data are displayed. The radial scale indicates relative frequency of observations. Alignment between wind and tidal direction resulted in a more uniform flow, while opposition introduced greater variability
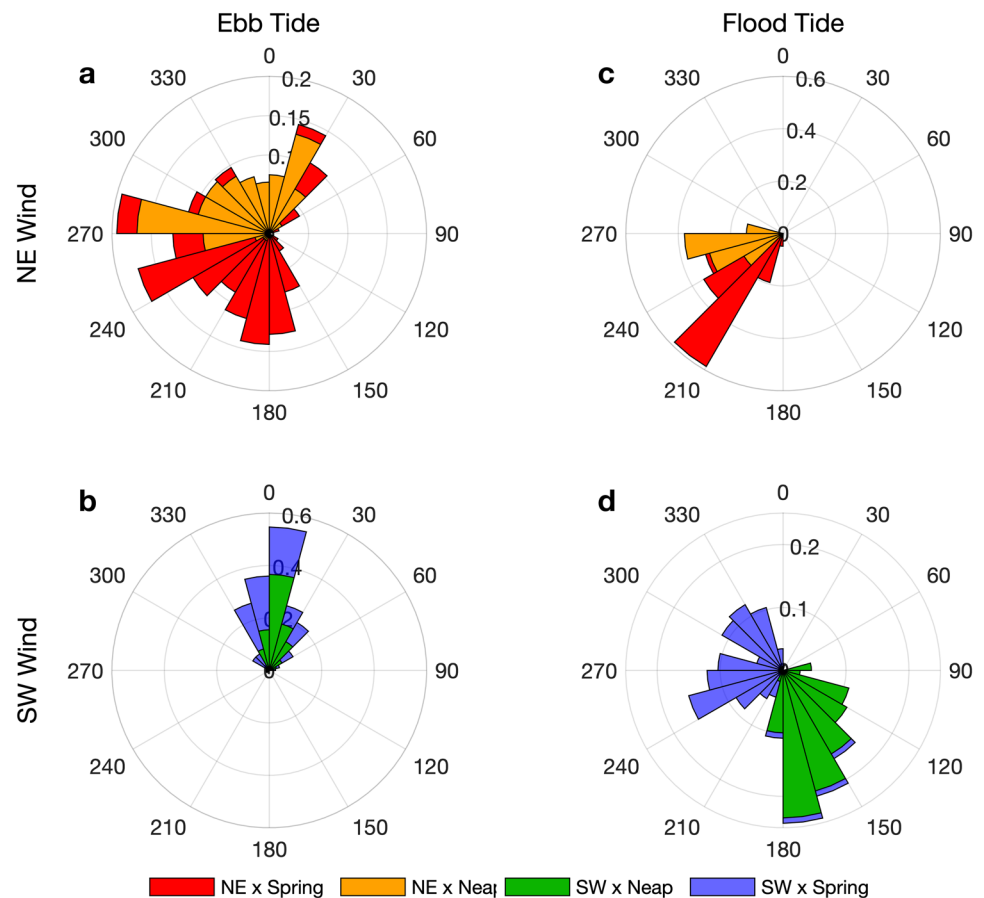
with the wind direction or typical flood transport observed in drifter deployments (detailed below).
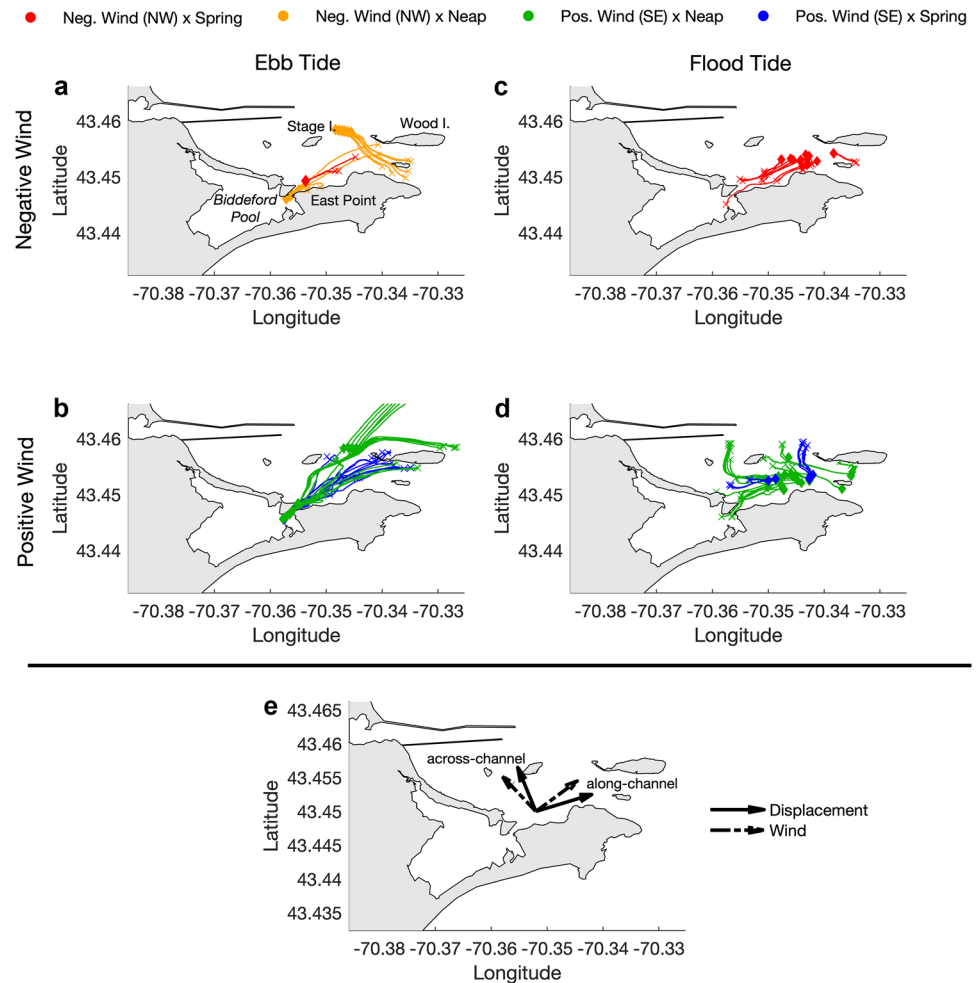
Drifter Deployments

Over 22 days, 119 individual drifter releases and recoveries were conducted, comprising 25 deployments. These deployments achieved coverage across the 8 conditions of different tidal directions (ebb and flood), tidal ranges (spring and neap), and along-channel wind directions (northeasterly and southwesterly) that were targeted. When considering the flow trajectories recorded across all drifter deployments (Fig. 4a–d), a coarse pattern in current direction was observed. A majority of flow appeared to occur along a line with roughly the same orientation as the Biddeford Pool inlet. We sought to estimate the orientation of that axis in order to describe transport in the context of along- and across-channel components. Simple linear regression was performed on the full set of points recorded by all drifters, as well as subsets of data to ensure the axis was robustly representing surface transport. These results, combined with the regression analyses detailed below, led to the definition of the along-channel axis as 70° and the across-channel axis as 340° (Fig. 4e). To identify the wind direction that had the greatest influence on

each component of displacement, regression analyses were repeated on wind components at 10° intervals and found that winds on 50° and 320° axes yielded relationships with the greatest R^2 values. For simplicity, these are referred to here as along- and across-channel winds, respectively. For both displacement and wind velocity components, positive values correspond with flow in the direction of that axis (i.e., a positive displacement or wind on the along-channel (across-channel) axis represents approximately northeastward (north-westward) flow).

Since wind on the across-channel axis proved to be more informative of drifters' behavior (detailed below), drifter tracks presented in Fig. 4 are divided between positive and negative winds on that axis, as well as the tidal conditions targeted (spring or neap and ebb or flood). Whereas drifter deployments encompassed a wide range of wind directions, UAV flights were specifically planned around along-channel wind conditions. Therefore, they were not re-classified. Since this classification was post hoc and not used when planning deployments, the number of deployments associated with each condition was more variable than originally intended, with some combinations of conditions having minimal or no coverage. Flood tide deployments were initiated from the offshore edge of Wood Island Harbor, based on expected

Fig. 4 Drifter tracks through Wood Island Harbor, grouped by northwesterly/negative across-channel wind (upper panels) and southeasterly/positive across-channel wind (lower panels) and flood (right panels) and ebb (left panels) tidal direction, and colored by spring and neap tidal range. Starting (ending) locations are indicated by a diamond (X). The final panel **e** is a conceptual figure showing the along- and across-channel axes used for drifter displacement and wind velocity in the regression analyses

trajectories into Biddeford Pool. Ebb tide deployments were initiated from the Biddeford Pool inlet, with the exception of 2 days, when 6 drifters were released along a line between Stage and Wood Islands to attain coverage in this area under different wind conditions.

Examination of the drifter trajectories revealed some common patterns within combinations of wind and tidal conditions. Ebb transport out of Biddeford Pool under negative across-channel (northwesterly) winds (Fig. 4a, n = 14) was associated with smaller displacements than under positive across-channel (southeasterly) winds (Fig. 4b, n = 42). Variations in tidal range did not produce differences in ebb drifter tracks under northwesterly winds; transport out of Biddeford Pool was generally restricted to the nearshore margin of Wood Island Harbor. Ebb trajectories exhibited greater variability and differences between spring and neap tides when positive across-channel winds were present. Except for one drifter, spring tide trajectories followed a common pathway along the channel axis, before grounding on or flowing to the south of Wood Island. Several drifters deployed during neap tides followed a similar path, while others had a greater positive component of across-channel

displacement, exiting the harbor between Stage and Wood Islands. Ebb transport in the northern portion of the harbor, assessed through deployments on the Stage Island to Wood Island line, significantly differed based on wind direction, with across-channel transport components aligned with the direction of across-channel winds.

Drifters deployed during flood tides showed greater variability in surface transport trajectories across wind directions. Negative across-channel (northwesterly) winds (Fig. 4c, n = 18) were associated with almost all drifters tracking towards Biddeford Pool. The effects of tidal range could not be considered, as all deployments occurred under spring tides. As with ebb tidal transport, positive across-channel (southeasterly) winds were associated with more variable drifter trajectories (Fig. 4d, n = 45). Although deployed in similar locations, drifter trajectories diverged in the harbor, with flow towards both Biddeford Pool and the Saco River. This pattern is consistent with the UAV observations of flood tidal flow under opposing along-channel winds. Drifters that were released in the northern half of the harbor or in the area between Wood Island and the mainland consistently traveled westward and northward, suggesting that the

division of flow between Biddeford Pool and the Saco River was robust. The one day that drifters were deployed during a flood spring tide, all observed flow was towards the Saco River. However, the strongest across-channel winds recorded for flood tide deployments occurred on this day, providing a confounding influence to assessing the effects of tidal range on flood tide trajectories.

Current velocities calculated from drifter data (not shown) were governed by tidal range and direction, wind direction, and bathymetry of the area. Across all sets of conditions, maximum velocities were recorded within the constriction separating Biddeford Pool from Wood Island Harbor, and current speeds decreased with distance from the inlet. Spring tides and alignment between tidal and wind direction also increased surface velocities. Magnitudes of typical ebb currents were 0.2–0.7 m s^{-1} through the majority of the harbor and 1.0–1.5 m s^{-1} in the inlet, peaking at 2.5 m s^{-1} under spring tides and southeasterly winds. Increased surface velocities (0.5–0.7 m s^{-1}) were also recorded for drifters that traveled in deeper water to the north of Wood Island.

Drifters passed through the Biddeford Pool inlet less frequently during flood tide deployments, but similar patterns still emerged. Velocity magnitudes through the inlet were 0.6–1.0 m s^{-1} under southeasterly winds but reached 1.8 m s^{-1} under northwesterly winds. Across all conditions, currents through the majority of Wood Island Harbor flowed at speeds of 0.1–0.4 m s^{-1}. Flood flow through the deep passage between Stage and Wood Islands under southeasterly winds was characterized by greater velocities (~0.5 m s^{-1}), relative to the main harbor. The slowest velocities (~0.1 m s^{-1}) were recorded along the harbor's shallow margins and near obstructions like intertidal rocks.

To identify and quantify the mechanisms producing the observed patterns of flow, we assessed correlations between displacement components and the environmental variables measured during each deployment. These analyses were performed on the averaged values for each deployment ($n=25$), to mitigate the correlation in space and time between drifters released in the same deployment. Regressions of the explanatory factors against along- and across-channel displacements were repeated for along-channel axes of 65°, 70°, and 75°. These analyses yielded similar results in R^2 and p-values across the axis values tested, affirming the choice of a 70° along-channel axis and 340° across-channel axis (Fig. 4e). The results of the regressions using those axes are presented in Table 1.

Factors that had significant correlations with displacement components were first identified by testing whether the slopes calculated in regression analysis differed from zero. R^2 values were then used to compare the explanatory power of factors with significant slopes. The regression analyses for individual variables were repeated for average along- and

Table 1 All individual relationships evaluated between environmental variables and displacement components. Coefficients of determination (R^2) and p-values from regression analysis are presented for each relationship. The environmental variable associated with the greatest significance and R^2 value for each component of displacement is shown in bold type. Sample size for each explanatory variable is also listed, as availability of environmental data was variable across drifter deployments

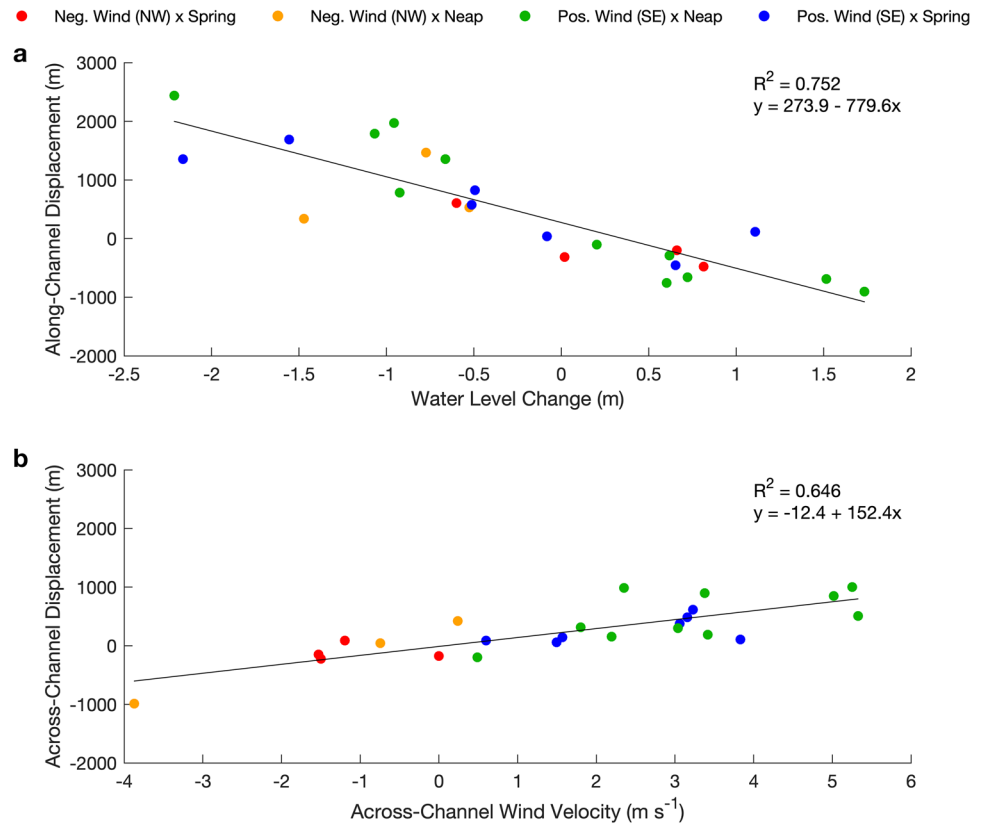| Explanatory variable	Along-channel displacement		Across-channel displacement	
	R^2	p	R^2	p
River discharge ($n=25$)	0.012	0.609	0.007	0.686
Water level change ($n=25$)	**0.752**	**< 0.0001**	0.019	0.506
Along-channel wind velocity ($n=24$)	0.074	0.199	0.286	0.007
Across-channel wind velocity ($n=24$)	0.023	0.478	**0.646**	**< 0.0001**
Significant wave height ($n=21$)	0.003	0.808	0.044	0.362
Mean wave direction ($n=21$)	0.028	0.466	0.002	0.846

across-channel current velocities. These returned the same significant factors, but with lower explanatory power.

For along-channel displacement, water level change (Fig. 5a) was the only variable to show significance across all tested values of the major axis. That relationship also had the highest R^2 value (0.752) among all factors evaluated.

Across-channel wind velocity had the strongest relationship ($R^2 = 0.646$) with across-channel displacement (Fig. 5b). In contrast to displacement along the channel axis, a second factor, along-channel wind velocity, showed a consistently significant relationship with across-channel displacement, though with a reduced R^2 value (0.286).

Multiple linear regression models were fitted to explore the main and interactive effects of sets of variables on each displacement component. These models were based on a smaller subset of deployments ($n=21$), as they incorporated wave parameters, which were not available from NDBC Station 44007 for all deployments. To provide for accurate comparisons, the regression analyses were repeated for the above models that used only wind velocities ($n=24$) or water level ($n=25$) using the reduced set of drifter data ($n=21$). This resulted in a reduction in R^2 values for both along-channel displacement as a function of water level change ($R^2 = 0.703$ vs. 0.752) and across-channel displacement as a function of across-channel winds ($R^2 = 0.525$ vs. 0.646). A model of along-channel displacement as a function of the 6 main effects in Table 1 showed change in water level had a significant effect, with along-channel wind showing marginal significance. An interactive model was then fitted, incorporating these two

Fig. 5 Scatterplots of the most explanatory environmental variable for each component of displacement, averaged by deployment. Along-channel displacement is plotted against water level change (**a**), and across-channel displacement is plotted against the across-channel component of wind velocity (**b**). Data points are colored by the wind direction and tidal range of their respective deployment

variables. This model showed significant main effects of both factors and a greater explanatory power ($R^2 = 0.855$). When a multiple regression model with all six main effects was fitted for across-channel displacement ($R^2 = 0.573$), across-channel wind velocity was the only factor with a significant effect. We fitted a second model that included the main effects of the variables found to have individually significant relationships with across-channel displacement (Table 1): along- and across-channel wind velocity components. The explanatory power of this model ($R^2 = 0.652$) was comparable to the original regression of orthogonal displacement and the across-channel wind velocity component ($R^2 = 0.646$).

Examining the range in displacement values for the parallel and orthogonal components (Fig. 5) revealed that along-channel displacement (−900 to 2400 m) was up to twice as much as across-channel displacement (−1000 to 1000 m). The largest negative across-channel displacements were recorded in a single deployment day; typical values were greater than −500 m.

To illustrate the explanatory capability of the environmental variables that showed the strongest individual relationships with displacement components, we developed a simple linear model of flow across the harbor. The water level change (m) and across-channel wind velocity component (m s⁻¹) during the time period of interest were used

as inputs to calculate displacement components and the total displacement (m).

$$d_{along} = 273.91 - 779.59 \times \Delta water\ level$$

$$d_{across} = -12.38 + 152.43 \times wind\ velocity_{across}$$

$$d_{total} = \sqrt{d_{along}^2 + d_{across}^2}$$

These values were transformed back to a standard coordinate system, converted to displacements in degrees of longitude and latitude, and then joined with the starting location within Wood Island Harbor to calculate the terminal location for a water parcel at the end of the time period. The full model equations are provided in the Online Resource. To evaluate this model, we applied it to the starting locations and environmental conditions for all drifter deployments we conducted. The actual recovery locations (red circles) are plotted in Fig. 6, along with the recovery locations calculated with the model (blue circles).

Although not intended to predict individual trajectories, the model produced results that were consistent with the drifter observations. No geographic constraints were included in our predictions, resulting in some calculated locations that were on, or crossed over, land. However, most

Fig. 6 Actual (red circles) and calculated (blue circles) recovery locations based on model of displacement for ebb and flood tide (**a**, **b**). Lines connect pairs of points corresponding to the actual and modeled recovery locations of a single drifter release. Distributions of actual drifter displacements (**c**) and model residuals (**d**) show relative performance of the model
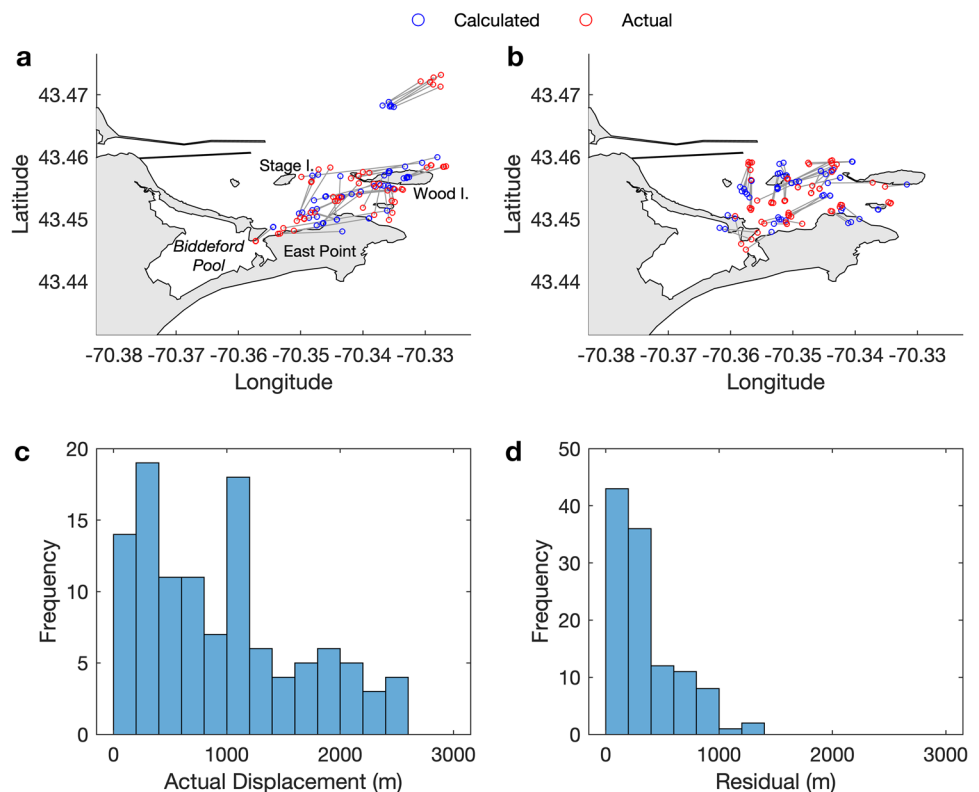
errors (Fig. 6d) were small relative to the actual track length (Fig. 6c). Inconsistencies between actual and calculated recovery locations were more notable for two sets of ebb tide deployments. Instead of the fast export away from the inlet observed for the majority of drifters, these seven tracks showed recirculation of surface waters on the harbor side of the inlet. This pattern of flow was captured under both positive (*n* = 3 drifters) and negative (*n* = 4 drifters) across-channel winds. After proceeding out of the inlet, drifters circulated through the area before eventually proceeding beyond the mouth of Biddeford Pool.

Discussion

Overview

Our observations of flow revealed complex patterns of surface currents that were influenced by multiple interacting mechanisms and varied in both space and time. However, the dynamics of individual topographic features were largely maintained, allowing us to describe flow patterns using simple linear models. These results allowed us to answer questions about exchange in the local context and describe generalized characteristics of flow around a topographically complex system with interactive, sometimes competing, forcings. UAV imagery revealed the temporal evolution

of transport patterns between high and low tides. During slack tide, current directions were uniform and appeared to be governed by wind stress. If the tidal direction and wind direction were aligned, this uniformity would typically persist. However, when the two forcings were opposed, spatial differences emerged in the current direction as tidal velocities increased, often in association with bathymetric features in the harbor. Transport within the channel demonstrated more consistent patterns across tidal range and wind direction, whereas flow over the shallow areas of the harbor exhibited greater variability.

Analyzing the drifter data revealed unifying characteristics of flow across all conditions sampled. The most significant was a common major axis of flow through the harbor, approximately oriented with the channel. Motion through the harbor could be decoupled into components parallel and orthogonal to this axis, and these displacement values were used to determine the most significant mechanisms governing surface flow. We identified a single factor with high explanatory power for each axis of flow. Additionally, analysis of drifter tracks in reference to the depth and contours of the harbor suggested bathymetric influences on surface transport. Spatial variability and smaller-scale flow features observed in both drifter and UAV data were also evident characteristics of surface currents through the area.

Tidal flow was the primary driver of along-channel transport through the harbor. Displacements along this axis were

typically greater than across-channel displacements, indicating water level change produced by tides had the greatest effect determining surface transport overall. With limited freshwater input and a shallow basin that is intertidal across most of its area (USACE 2020a), it was expected that tidal flow would be the dominant influence on surface transport in and around Biddeford Pool. The regression analysis of water level change against along-channel displacement allowed tidal range to be considered with tidal direction. The negative correlation across deployment-averaged drifter data supported that spring tides are associated with larger displacements (Zarzuelo et al. 2017; de Ruiter et al. 2019).

Wind stress was also identified as a significant mechanism affecting flow, but its influence was contrary to expectations. Based upon previous studies of the area, along-channel winds were predicted to be most influential on surface flow (Tilburg et al. 2011; Fortier 2014). When incorporated in a multiple regression model with water level change, along-channel (50°) winds were a significant factor governing along-channel transport. However, the inclusion of the wind component and its interaction with water level change provided only a modest increase in explanatory power ($R^2 = 0.855$) as compared to the univariate regression model ($R^2 = 0.752$). Therefore, we recognize that along-channel wind velocity influenced parallel displacement and interacted with water level change, although its contributions were small compared to the tidal forcing.

The across-channel (320°) component of wind velocity was found to be much more relevant, explaining a majority of across-channel displacement ($R^2 = 0.646$). Examination of flow trajectories from both drifter and UAV sampling suggested the influence of winds differed spatially and interacted

with tidal flow. Current direction distributions captured with the UAV showed increased effects of wind during slack tide. Along-channel wind velocity also had a significant individual relationship with across-channel displacement, though with reduced explanatory power ($R^2 = 0.286$). Based upon its lesser influence and the lack of significant effects in the multiple regression models of across-channel displacement, it was omitted from our simple model of surface transport.

In contrast with previous investigations of flow dynamics through dredged channels (e.g., Chen et al. 2015; Moulton et al. 2017), we observed a decreased effect of wave energy on surface transport within the study area. The topographic setting of the harbor-inlet system likely interacted with wave conditions to moderate their effect. Mean wave direction during deployments ranged from 90° to 200°, meaning that the East Point tombolo would shield the region from direct wave impacts, as documented by Kelley et al. (2005). A reduction in wave energy reaching the area would reduce the momentum transfer to surface currents (Tang et al. 2007).

Local Dynamics

Our determination of the primary mechanisms operating in the area, coupled with the intricacies of flow observed under particular conditions, allowed us to describe circulation within the local context. Transport out of Biddeford Pool during ebb tides (Fig. 7a) was consistently directed offshore through Wood Island Harbor and concentrated in the deep channel. The channel operated as a linked system with the Biddeford Pool inlet, likely reducing attenuation of the flow typically found moving away from a constricted inlet (Baines 1957; Maas 1997; de Ruiter et al. 2019). The uniformity
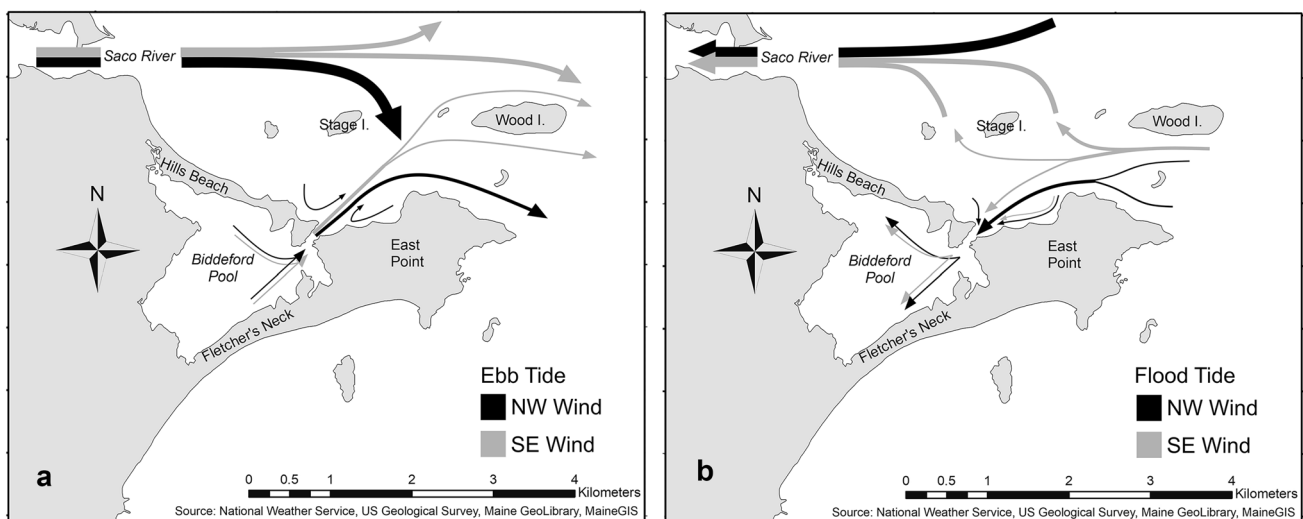

Fig. 7 Flow trajectories through southern Saco Bay, based on aggregated results. Patterns of flow are divided between ebb tide (**a**) and flood tide (**b**), as well as northwesterly and southeasterly winds

of this area's higher-velocity flow was consistent with the strong ebb jet that exits a constricted-inlet basin (Lee et al. 2013; Rynne et al. 2016) and a low effect of along-channel winds. Across-channel (320°) winds were more relevant, with northwesterly winds restricting ebb progress and southeasterly winds resulting in greater offshore transport.

While there was coherence between UAV and drifter-based observations of flow in the channel, visual analysis revealed differences in flow trajectories between other areas of the harbor, governed by bathymetry. Drifter trajectories showed recirculation of surface waters near the inlet during the ebb tide, in contrast to the consistent offshore-directed flow through the channel. The direction of transport appeared to be influenced more by wind stress over shallow areas of the harbor. Ebb flow under along-channel winds from offshore showed wind-aligned flow in the western harbor, presenting a possible mechanism for water from the Saco River plume to enter Biddeford Pool. In deeper water, transport tended to follow the contours of the seafloor in the harbor channel and between the islands separating the harbor from Saco Bay. Drifters released at the basin inlet would follow the eastward curvature of the channel when exiting the harbor, before diverting to either side of Wood Island. Topographic effects were also noted to the north of Wood Island, where a shallow ledge bifurcated surface flow. These deep passages facilitated faster transport and offshore export of ebb flows, as did southwesterly winds.

Examination of transport patterns during the flood tide revealed how the local system participates in the larger context of Saco Bay's circulation (Fig. 7b). Moore et al. (2020) discussed an anticyclonic gyre through Saco Bay, with northward transport close to shore. As water enters the area from offshore, flow is divided through the harbor (e.g., Fig. 2d), likely following deeper bathymetry. The flood currents coming through the passage south of Wood Island and turning northward represent the inflow of water to the Saco River and nearshore circulation of the bay. Through the southern portion of the harbor, water is entrained from this westward flow to fill Biddeford Pool. This process was evidence of the influence of the Saco River on current patterns through Wood Island Harbor, though not in the way that was expected. The Saco River estuary's saltwater tidal prism of 8.1×10^6 m^3 (FitzGerald et al. 1989) is nearly twice that of Biddeford Pool's 4.5×10^6 m^3 tidal prism (Pixa 2017 [unpublished data]), making it a significant sink for waters in southern Saco Bay during the flood tide. As a result, flow through the northern region of Wood Island Harbor is directed towards the river and does not enter Biddeford Pool as originally expected.

The spatial variation in flood transport direction was largely consistent across wind direction and tidal range; negative across-channel (northwesterly) winds were associated with a slight expansion of the portion of Wood Island Harbor that flowed into Biddeford Pool. UAV-based observations of flood flow under opposing along-channel winds showed that the harbor's division of flow was maintained, rather than surface currents becoming aligned with the wind direction. We propose that the reduced fetch of southwesterly winds results in a diminished influence when opposed to the tidally driven flow. Comparisons between distributions of flow direction under spring and neap tides (Fig. 3d) indicated that the influence of wind on surface transport may be more pronounced at reduced tidal ranges, since the typical pattern was not seen during neap tides.

In addition to patterns in the direction of surface transport, differences emerged in current velocity both spatially and across the sets of wind and tidal conditions we tested. Greater current speeds were recorded in deeper waters like the channel and inter-island passages, as compared to the shallow areas of the harbor. Increased tidal range was also associated with increased velocities in the channel, as was found by Zarzuelo et al. (2017) and de Ruiter et al. (2019). However, flood current velocities in the inlet and Wood Island Harbor were reduced across all conditions compared to the ebb currents. This reduction can be attributed to the dynamics of constricted-inlet systems, as deep channels tend to be ebb-dominated, even if the basin as a whole is not (Stanev et al. 2007; Hunt et al. 2016; de Ruiter et al. 2019). During the flood tide, water is drawn in from a broad area around the inlet, and flow is less energetic than in the high-velocity jet of the ebb tide (Rynne et al. 2016). Within the basin, flood current velocities are greater near the inlet, as the focused flow enters the area.

As Biddeford Pool empties on the ebb tide, two main possibilities exist for the fate of the discharge. Under positive across-channel winds, water is efficiently exported from Wood Island Harbor through the combined effects of the ebb jet, dredged channel, and inter-island passages. A few drifters that could not be recovered at the end of their deployment and ultimately reached the northern end of Saco Bay revealed that flow can continue northward, oscillating east and west with the tide. Outflow from the basin close to slack tide is expected to return on the subsequent flood tide, as the ebb jet diminishes in strength and flow does not exit the area that drains into the Pool. This retention of water is expected to occur more reliably under negative across-channel (northwesterly) winds, when ebb progress is constrained. While not directly observed, the Saco River plume would be most likely to mix with water filling Biddeford Pool under these conditions. Winds, therefore, exert a significant influence on the degree of renewal of Biddeford Pool water over successive tide cycles.

Coherence with Flow Parameters

The patterns of surface flow and most relevant mechanisms identified in the area were consistent with the non-dimensional parameters calculated to describe flow through the inlet and the

harbor. Please consult the Online Resource for equations and the distance and velocity scales chosen for their calculation. Large Rossby (~ 100) and temporal Rossby (~ 15) numbers indicated a system dominated by local advection. The spatial scale of the flow that we considered was similar or reduced relative to previous studies of other constricted-inlet systems (Zarzuelo et al. 2017; de Ruiter et al. 2019). Therefore, it is expected that we did not find rotationally dominated flow, given that these past studies did not observe rotational effects either. Tilburg et al. (2011) only found rotational effects in the region under high discharge from the Saco River, when the spatial scale of the plume (10 km) was greater than that of the flow (2 km) we studied. The relationship between wind velocity components and displacement supports a limited influence of rotational processes, as transport was neither directly downwind nor shifted 45° from the wind, as would be expected in a rotational system. The combined evidence of insignificant rotational processes (large Rossby number), varied bathymetry, and flow along bathymetric contours allows for the attribution of flow features like the eastward deflection of the ebb jet to the effects of bathymetry and not Coriolis forces.

High values of Ekman (140) and Reynolds (20,000) numbers for flows near the inlet indicated a friction-dominated, turbulent system. These values are consistent with the typical dynamics of constricted-inlet systems. As high-velocity flow passes through a constricted inlet, the resulting horizontal shear produces turbulence and eddies downstream (Krüger and Healy 2006; Lee et al. 2013; Zarzuelo et al. 2017; de Ruiter et al. 2019). While eddy-type circulation was observed anecdotally, additional targeted sampling would be necessary to assess shear and turbulence associated with the inlet system. Similarly, the Reynolds number (3000) for the harbor indicated turbulent flow; however, shear is likely reduced relative to the inlet, as the entrances to the harbor are more open, leading to a weaker velocity gradient. Again, a subsequent investigation would be required to characterize shear or turbulence within the system examined here.

Modeling

Despite the complex, interactive physical mechanisms and bathymetric influences apparent in the Biddeford Pool-Wood Island Harbor system, a simple model proved effective in representing flow through the area. The coherence between our observations and the model results strongly supported the importance of water level change and across-channel wind velocity influencing patterns of surface transport. We acknowledge that the flow dynamics of an area cannot be attributed to one or two isolated mechanisms; surface current patterns are the combined result of many interacting factors. However, the benefits realized from including additional main and interactive effects in a regression model of along-channel displacement were small in this case, considering the explanatory power of water level change alone. This result suggests that the use of a linear model to examine multiple features may be useful in other studies of coastal transport.

Even without topographic bounds, predicted trajectories were largely limited to the harbor area, and the model performed well across the range of wind and tidal conditions in which we sampled. A notable exception was observed in some ebb tide trajectories (Fig. 6a) that corresponded to drifters that recirculated close to the inlet. Therefore, despite being deployed for several hours and traveling a large total distance, their actual net displacements were small. If this model was to be used to forecast displacement through the area, significant modifications would be necessary. In addition to having more complete coverage through the area, the model would need to include the influence of a broader range of forcing conditions. The model would also need to be trained for the differences in velocity and displacement that emerge over smaller spatial and temporal scales; such a model would require topographic and bathymetric constraints as well.

Limitations

Our ability to fully characterize the influence of some mechanisms or describe the complete scope of flow patterns was constrained in some areas. Our ability to describe the influence of river discharge and seasonality on surface currents was limited by the temporary cessation of research activities during the 2020 spring freshet. Sampling during the spring would most likely reveal both the direct influence of the Saco River plume and a connection with the WMCC, as the river plume would draw water eastward from the harbor. Additionally, the lack of wind and wave observations from directly within the study area constrained our ability to account for smaller-scale variations that would be expected in a topographically complex system.

The post hoc classification of drifter deployments by across-channel wind direction resulted in unequal coverage between sets of conditions. Additionally, limiting the categories to 2 main wind directions to visualize data and identify preliminary patterns introduced variability within each grouping. However, the calculation of separate wind components when assessing mechanisms producing transport mitigated this issue. Temporal variability in velocities and spatial variability in flow trajectories were under-covered in drifter deployments under some conditions. All ebb drifter deployments originated within or near the inlet, and tracks in the southern area of the harbor were restricted to the channel. As a result, ebb flow through the western part of the harbor was not well assessed. This lack of sampling left us unable to corroborate the patterns of wind-driven surface flow evident in UAV data recorded under northeasterly

winds. Lastly, a description of exchange through this system would require sampling through the full water column, which was beyond the scope of this study. These data would also allow for the quantification of bathymetric effects like bottom friction, a significant mechanism in energy dissipation through channels and constricted inlets (Zarzuelo et al. 2017). The importance of bathymetry in governing flow could then be assessed relative to the influences of wind velocity and tidal phase.

Next Steps

When examining flow through a complex system of a constricted-inlet basin, dredged channel, and islands surrounding a harbor, we found surface transport was influenced by a few dominant factors. The linked inlet and channel served as a major conduit of flow through the harbor, as transport followed bathymetric contours. Along the channel axis, transport was tidally driven, with deviations in trajectories governed primarily by across-channel winds. The presence of a large estuary adjacent to the harbor introduced an additional sink for discharge from the constricted-inlet basin as it was entrained by larger-scale circulation patterns of the bay.

Both the findings and limitations of our study invite further investigation on a local and general level. The apparent ability of Biddeford Pool to exchange its waters over a tidal cycle suggests that internal sources of microbial pollution may have greater impacts on the water quality of a constricted-inlet basin. Measuring currents within Biddeford Pool would also be necessary to describe the spatial variability in residence time that characterizes constricted-inlet basins (Brooks 2004; Rynne et al. 2016; Viero and Defina 2016). The completed USACE dredging project also merits a follow-up investigation of flow through the channel. The dredged area now extends a greater distance from Biddeford Pool and meets with the previous channel before it curves eastward. A greater northward component of flow could conceivably enhance the export of water on the ebb tide, increasing the rate of renewal in Biddeford Pool. The linkage between Biddeford Pool and the circulation through Saco Bay also merits additional study, using longer-term drifter deployments to expand our findings of northward movement along the coast. Towards the aim of describing flow through an interconnected system of a constricted-inlet basin, dredged channel, and inter-island passages, the data we collected could serve as inputs or validation for a numerical model. A more generalized representation of flow could be derived from such a model and manipulated to evaluate the effects of local conditions and lower-order mechanisms that we found to have marginal significance or low explanatory power.

References

Baines, W.D. 1957. Tidal currents in constricted inlets. *Coastal Engineering Proceedings* 6: 545–561.

Benassai, G., P. Aucelli, G. Budillon, M. De Stefano, D. Di Luccio, G. Di Paola, R. Montella, L. Mucerino, M. Sica, and M. Pennetta. 2017. Rip current evidence by hydrodynamic simulations, bathymetric surveys and UAV observations. *Natural Hazards and Earth System Sciences* 17 (9): 1493.

Bigelow, H.B. 1927. *Physical oceanography of the Gulf of Maine (No. 969)*. Washington, D.C.: US Government Printing Office.

Brooks, D.A. 2004. Modeling tidal circulation and exchange in Cobscook Bay. *Maine. Northeastern Naturalist* 11 (sp2): 23–50.

Brothers, L.L., D.F. Belknap, J.T. Kelley, and C.D. Janzen. 2008. Sediment transport and dispersion in a cool-temperate estuary and embayment, Saco River estuary, Maine, USA. *Marine Geology* 251 (3–4): 183–194.

Chen, J.-L., T.-J. Hsu, F. Shi, B. Raubenheimer, and S. Elgar. 2015. Hydrodynamic and sediment transport modeling of New River Inlet (NC) under the interaction of tides and waves. *Journal of Geophysical Research: Oceans* 120 (6): 4028–4047.

Churchill, J.H., N.R. Pettigrew, and R.P. Signell. 2005. Structure and variability of the Western Maine Coastal Current. *Deep-Sea Research Part II* 52 (19–21): 2392–2410.

Dérian, P., and R. Almar. 2017. Wavelet-based optical flow estimation of instant surface currents from shore-based and UAV videos. *IEEE Transactions on Geoscience and Remote Sensing* 55 (10): 5790–5797.

de Ruiter, P.J., J.C. Mullarney, K.R. Bryan, and C. Winter. 2019. The links between entrance geometry, hypsometry and hydrodynamics in shallow tidally dominated basins. *Earth Surface Processes and Landforms* 44 (10): 1957–1972.

DiLorenzo, J.L., E. Hasbrouck, and T.O. Najarain. 1995. Water quality screening method for a coastal boat basin. *WIT Transactions on the Built Environment* 9: 151–160.

FitzGerald, D.M., J.M. Lincoln, L.K. Fink, and D.W. Caldwell. 1989. Morphodynamics of tidal inlet systems in Maine. In *Studies in Maine geology: Volume 5 - Quaternary geology*, eds. R. D. Tucker, and R. D. Marvinney, 67–96. Augusta, ME: Maine Geological Survey.

Fortier, B.A. 2014. *The Saco River plume: A discussion of the near-field dynamics*. Biddeford, ME: University of New England.

Geyer, W.R., R.P. Signell, D.A. Fong, J. Wang, D.M. Anderson, and B.A. Keafer. 2004. The freshwater transport and dynamics of the Western Maine Coastal Current. *Continental Shelf Research* 24 (12): 1339–1357.

Graham, G. 2019. Mysterious Biddeford Pool pollution forces thee-month shellfish closure. Portland Press Herald. https://www.pressherald.com/2019/09/30/mysterious-biddeford-pool-pollution-forces-three-month-shellfish-closure/. Accessed 24 June 2021.

Hamner, W.M., and I.R. Hauri. 1977. Fine-scale surface currents in the Whitsunday Islands, Queensland, Australia: Effect of tide and topography. *Marine and Freshwater Research* 28 (3): 333–359.

Hill, H.W., J.T. Kelley, D.F. Belknap, and S.M. Dickson. 2004. The effects of storms and storm-generated currents on sand beaches in Southern Maine, USA. *Marine Geology* 210 (1–4): 149–168.

Hollyhead, C.J., N.C. Townsend, and J.I. Blake. 2017. Experimental investigations into the current-induced motion of a lifeboat at a single point mooring. *Ocean Engineering* 146: 192–201.

Hunt, S., K.R. Bryan, J.C. Mullarney, and M. Pritchard. 2016. Observations of asymmetry in contrasting wave- and tidally-dominated environments within a mesotidal basin: Implications for estuarine morphological evolution. *Earth Surface Processes and Landforms* 41 (15): 2207–2222.

Kelley, J.T., D.C. Barber, D.F. Belknap, D.M. FitzGerald, S. van Heteren, and S.M. Dickson. 2005. Sand budgets at geological, historical and contemporary time scales for a developed beach system, Saco Bay, Maine, USA. *Marine Geology* 214 (1–3): 117–142.

Krüger, J.C., and T.R. Healy. 2006. Mapping the morphology of a dredged ebb tidal delta, Tauranga Harbor, New Zealand. *Journal of Coastal Research* 22 (3): 720–727.

Lee, J., B.M. Webb, B. Dzwonkowski, K. Park, and A. Valle-Levinson. 2013. Bathymetric influences on tidal currents at the entrance to a highly stratified, shallow estuary. *Continental Shelf Research* 58: 1–11.

Maas, L.R. 1997. On the nonlinear Helmholtz response of almost-enclosed tidal basins with sloping bottoms. *Journal of Fluid Mechanics* 349: 361–380.

Maine Department of Marine Resources (DMR). 2020. 2007–2019 Maine soft clam landings by port. Augusta, ME: Maine DMR.

Moore, S., H. Xue, N.R. Pettigrew, and J. Cannon. 2020. Linear and nonlinear responses to northeasters coupled with sea level rise: a tale of two bays. In *Estuaries and coastal zones: dynamics and response to environmental changes*, eds. J. Pan, and A. Devlin. London: IntechOpen.

Moulton, M., S. Elgar, B. Raubenheimer, J.C. Warner, and N. Kumar. 2017. Rip currents and alongshore flows in single channels dredged in the surf zone. *Journal of Geophysical Research: Oceans* 122 (5): 3799–3816.

Paruch, L., A.M. Paruch, H.G. Eiken, and R. Sørheim. 2019. Faecal pollution affects abundance and diversity of aquatic microbial community in anthropo-zoogenically influenced lotic ecosystems. *Scientific Reports* 9: 19469.

Pettigrew, N.R., J.H. Churchill, C.D. Janzen, L.J. Mangum, R.P. Signell, A.C. Thomas, D.W. Townsend, J.P. Wallinga, and H. Xue. 2005. The kinematic and hydrographic structure of the Gulf of Maine Coastal Current. *Deep-Sea Research Part II* 52 (19–21): 2369–2391.

Ralston, D.K., and M.T. Stacey. 2006. Shear and turbulence production across subtidal channels. *Journal of Marine Research* 64 (1): 147–171.

Reynolds, W.W., and M.E. Casterlin. 1985. Vagile macrofauna and the hydrographic environment of the Saco River Estuary and adjacent waters of the Gulf of Maine. *Hydrobiologia* 128 (3): 207–215.

Robinson, A.R., M. Esty, and C.E. Tilburg. 2021. A compact GPS surface drifter with LoRa telemetry and self-contained tracking system. *Marine Technology Society Journal* 55 (1): 88–105.

Rynne, P., A. Reniers, J. van de Kreeke, and J. MacMahan. 2016. The effect of tidal exchange on residence time in a coastal embayment. *Estuarine and Coastal Shelf Science* 172: 108–120.

Signell, R.P., and W.R. Geyer. 1991. Transient eddy formation around headlands. *Journal of Geophysical Research: Oceans* 96 (C2): 2561–2575.

Stanev, E.V., G. Brink-Spalink, and J.O. Wolff. 2007. Sediment dynamics in tidally dominated environments controlled by transport and turbulence: A case study for the East Frisian Wadden Sea. *Journal of Geophysical Research: Oceans* 112 (C4): C04018.

Tang, C.L., W. Perrie, D. Jenkins, B.M. DeTracey, Y. Hu, B. Toulany, and P.C. Smith. 2007. Observation and modeling of surface currents on the Grand Banks: A study of the wave effects on surface currents. *Journal of Geophysical Research: Oceans* 112 (C10): C10025.

Tauro, F., A. Petroselli, and E. Arcangeletti. 2016. Assessment of drone-based surface flow observations. *Hydrological Processes* 30 (7): 1114–1130.

Tilburg, C.E., and R.W. Garvine. 2004. A simple model for coastal sea level prediction. *Weather and Forecasting* 19 (3): 511–519.

Tilburg, C.E., S.M. Gill, S.I. Zeeman, A.E. Carlson, T.W. Arienti, J.A. Eickhorst, and P.O. Yund. 2011. Characteristics of a shallow river plume: Observations from the Saco River Coastal Observing System. *Estuaries and Coasts* 34 (4): 785–799.

Tilburg, C.E., L.M. Jordan, A.E. Carlson, S.I. Zeeman, and P.O. Yund. 2015. The effects of precipitation, river discharge, land use and coastal circulation on water quality in coastal Maine. *Royal Society Open Science* 2 (7): 140429.

US Army Corps of Engineers (USACE). 2016. Saco Bay, Maine: sediment budget for late twentieth century to present. Vicksburg, MS: U.S. Army Engineer Research and Development Center.

US Army Corps of Engineers (USACE). 2020a. Environmental assessment, finding of no significant impact and Section 404(b)(1) evaluation for maintenance dredging: Wood Island Harbor and the Pool at Biddeford, Biddeford, Maine. Concord, MA: USACE New England District.

US Army Corps of Engineers (USACE). 2020b. Wood Island Harbor and the Pool at Biddeford, Biddeford, Maine maintenance dredging: drawings. Concord, MA: USACE New England District.

US Army Corps of Engineers (USACE). 2020c. Wood Island Harbor and the Pool at Biddeford, Biddeford, Maine maintenance dredging: construction solicitation and specifications. Concord, MA: USACE New England District.

van Heteren, S., D.M. FitzGerald, D.C. Barber, J.T. Kelley, and D.F. Belknap. 1996. Volumetric analysis of a new England barrier system using ground-penetrating radar and coring techniques. *The Journal of Geology* 104 (4): 471–483.

Viero, D.P., and A. Defina. 2016. Water age, exposure time, and local flushing time in semi-enclosed, tidal basins with negligible freshwater inflow. *Journal of Marine Systems* 156: 16–29.

Wang, J., H. Li, P. Li, and K. Zhou. 2007. Nonlinear coupled analysis of a single point mooring system. *Journal of Ocean University of China* 6 (3): 310–314.

Wolanski, E., J. Imberger, and M.L. Heron. 1984. Island wakes in shallow coastal waters. *Journal of Geophysical Research: Oceans* 89 (C6): 10553–10569.

Zarzuelo, C., A. López-Ruiz, M. Díez-Minguito, and M. Ortega-Sánchez. 2017. Tidal and subtidal hydrodynamics and energetics in a constricted estuary. *Estuarine and Coastal Shelf Science* 185: 55–68.